

DETERMINATION OF THE OPTIMAL MRI SEQUENCE FOR THE DETECTION OF MALIGNANT LUNG NODULES

W. Luboldt^{1,2}, A. Wetter¹, K. Eichler¹, T.J. Vogl¹, T.O.F. Wagner³, M.D. Seemann⁴

¹Department of Radiology, University of Frankfurt, Germany

²www.screening.info - Foundation

³Department of Internal Medicine, University of Frankfurt, Germany

⁴Department of Radiology and Nuclear Medicine, University of Magdeburg, Germany

Abstract

Objective: For staging, follow-up and even screening (www.screening.info) an "all-in-one" imaging examination is desirable. In the concept of whole body MRI, lung imaging prevails as the weakest link. The purpose of our study was to determine the optimal MRI sequences for the detection of malignant lung nodules.

Patients and Methods: On the basis of 6 lung cancer, 46 metastases and one tuberculoma in 13 patients eight MRI sequences - HASTE, IR-HASTE, fat saturated TrueFISP, STIR, VIBE_{ipat = 2}, and contrast-enhanced (CE) VIBE (with ipat = 2, 0, 4) performed with parallel imaging and 12 matrix coil elements - were compared in terms of contrast-to-noise ratio (CNR) and quality in the visualization of the lung nodules using multidetector CT as standard of reference. The parameters of the sequences were pragmatically selected to minimize the imaging time to allow for imaging the entire lung within one breathhold interval.

Results: The STIR sequence was found to be the best for detecting malignant lung nodules ($p < 0.01$) followed by the FS TrueFISP, CE VIBE_{ipat = 0}, CE VIBE_{ipat = 2}, IR-HASTE, HASTE, CE VIBE_{ipat = 4}, and VIBE. The STIR sequence visualized malignant nodules down to 2 mm in size and did not display the 19 mm tuberculoma.

Conclusion: The STIR sequence should be included in future studies investigating if MRI can compete with CT in the early identification (detection and classification) of malignant lung nodules.

Key words: MRI, STIR sequence, malignant lung nodules

INTRODUCTION

Parallel imaging technology [7, 9] is revolutionizing MRI much in the same fashion that multi detectors have improved CT. Currently, MRI technology features up to 32 radio-frequency channels and 76 matrix coil elements. This concept of total imaging matrix (TIM) allows for imaging the whole body without changing coils and subsequent repositioning of patients. Whole body MRI can now be performed "similarly" to multi-detector CT with data acquisition remaining as the only time-consuming step. For example, MR-mammography can easily be combined with lymph node, brain, lung, liver and bone imaging [4,

15]. Yet in the concept of whole body MRI, lung imaging prevails as the weakest link. Motion artifacts, caused by breathing and heart pulsations [2], and the relatively large volume to be imaged render lung MRI very challenging. In addition, MRI has to compete with CT [13], which is the standard of reference in lung imaging nearly since first being introduced in 1972. However, recent developments in MRI (volume interpolated breathhold examination and parallel imaging) are promising to improve lung MRI. The low content of protons in the normal, aerated lung, however, predestinates MRI for optimal depiction of lung malignancies based on their water content and/or on their contrast enhancement.

The purpose of our study was to determine the optimal MRI pulse sequence for the detection of malignant lung nodules and to compare its performance with CT.

PATIENTS AND METHODS

Thirteen consecutive patients (10 male, 3 female; aged 48-76, mean: 62 ± 8 years), who were newly diagnosed with lung nodules from plain radiographs and, thus, being referred for CT staging, underwent lung MRI within two days after CT. Six patients had primary lung cancer, six had multiple lung metastases (two from colon cancer, one from melanoma, one from squamous cell carcinoma of the neck, one from parotid cancer, one from thyroid cancer) and one patient had a 19 mm large tuberculoma. All lung cancer and the tuberculoma were histologically confirmed. The patients newly diagnosed with lung cancer had no previous radiation or chemotherapy, and the patients with the lung metastases had their last chemotherapy for the primary cancer more than a year ago.

Staging CT was performed on a 16-slice CT (Sensation, Siemens Medical Systems, Forchheim, Germany) in high spatial resolution, using: 120 kV, 120 effective mAs, 16 x 0.75 mm collimation, 24 mm / 0.5 s table feed, and a reconstruction increment of 0.5 mm. Immediately after the CT, each patient underwent lung MRI. Lung MRI was performed either in the frame of liver/bone MRI or because iodine contrast media could not be given as in the case of the patients with thyroid cancer or because the CT finding was unequivocal as in the case of the patients with the large (19 mm) tuberculoma. Informed consent was obtained

Table 1. Sequences tested for the detection of malignant lung nodules (Fig. 1 and 2).

	HASTE	IR-HASTE	TrueFISP	STIR	VIBE	contrast enhanced (CE)		VIBE
i-pat	2	2	2	2	2	2	0	4
Fat sat./TI	-	170 ms	+	150 ms	+			
CE					-	0.2 mmol/kg BW		
Delay					-	30 s	60 s	90 s
TR/TE [ms]	796/84	407/39	413/2.15	3540/120			2.84/1.16	
Flip	150°	160°	60°	150°			15°	
Matrix			256x80				256x75	
Slice-th.			4 mm				1.2-1.4 mm	
Slices		50		5 x 10	160		2 x 88	160
BW [Hz]	230	780	501	200			630	

HASTE = half-Fourier acquisition single-shot turbo spin-echo

IR-HASTE = inversion recovery HASTE

TrueFISP = true fast imaging with steady-state precession

STIR = short tau inversion recovery

VIBE = volumetric interpolated breath-hold examination

i-pat = integrated parallel acquisition technique

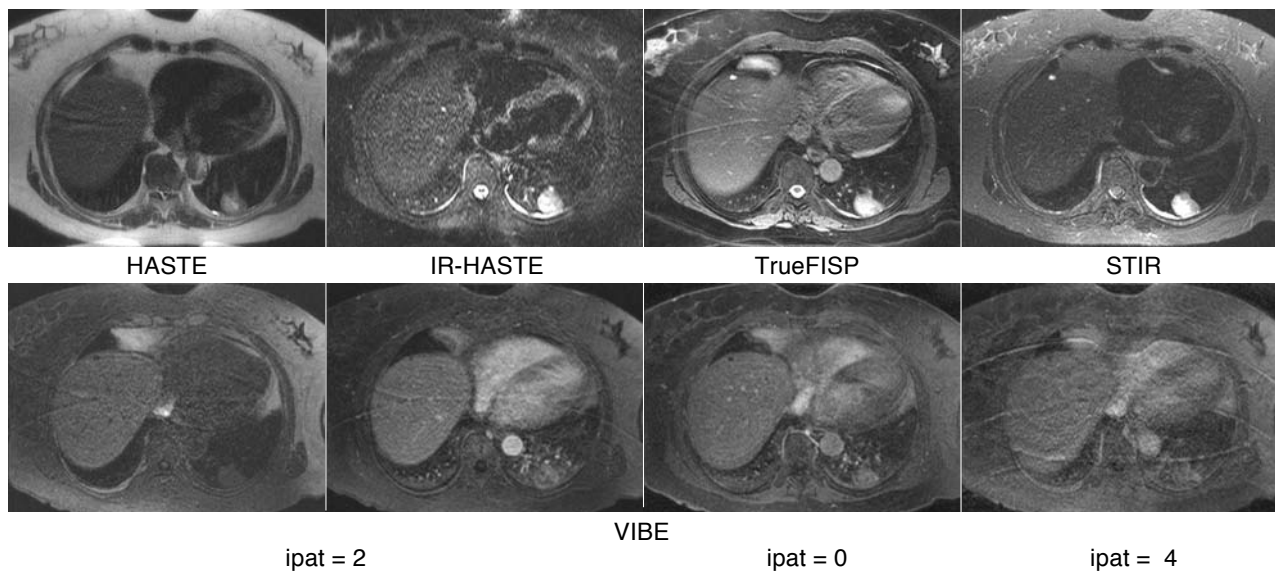


Fig. 1. Lung cancer (29 mm in size) in the left lower lobe. Comparison of different MRI sequences (Table 1). The STIR- and TrueFISP sequences showed the highest contrast-to-noise ratio (CNR), sensitivity and quality in the depiction of the lung cancer.

from all patients as set forth by the local ethic committee.

MRI was performed on a 1.5 T scanner (Sonata, Siemens Medical Systems, Erlangen, Germany) with parallel imaging, using 12 matrix coil elements. The scan protocol is summarized in Table 1 and illustrated in Figures 1 and 2. The sequence parameters were pragmatically selected to minimize the scan time in order to allow for imaging within the confine of one breathhold interval of 20 seconds. Only the short tau inversion recovery (STIR) sequence and the volume interpolated breathhold examination (VIBE) without parallel imaging (ipat = 0) needed to be performed in multiple (6 and 2) breathholds. The VIBE was performed before and three times after an IV bolus ad-

ministration of 0.2 mmol/kg BW gadopentetate dimeglumine (Magnevist, Schering, Berlin, Germany) with ipat = 2, 0, 4 (Table 1). The delay times were 30, 60, and 90 seconds.

Images were analyzed by two experienced radiologists in a consensus reading on a diagnostic workstation. Only the nodules with a clear correlate in the CT were included in the analysis (side-by-side comparison). The countless number of nodules < 3 mm in the patient with thyroid carcinoma as well as the many nodules > 5 mm in the patient with the parotid cancer (Fig. 2) were excluded to simplify the analysis. The signal intensity of the nodules, adjacent normal lung, and noise were determined by region-of-interest (ROI) measurements. The ROIs were manually placed. For

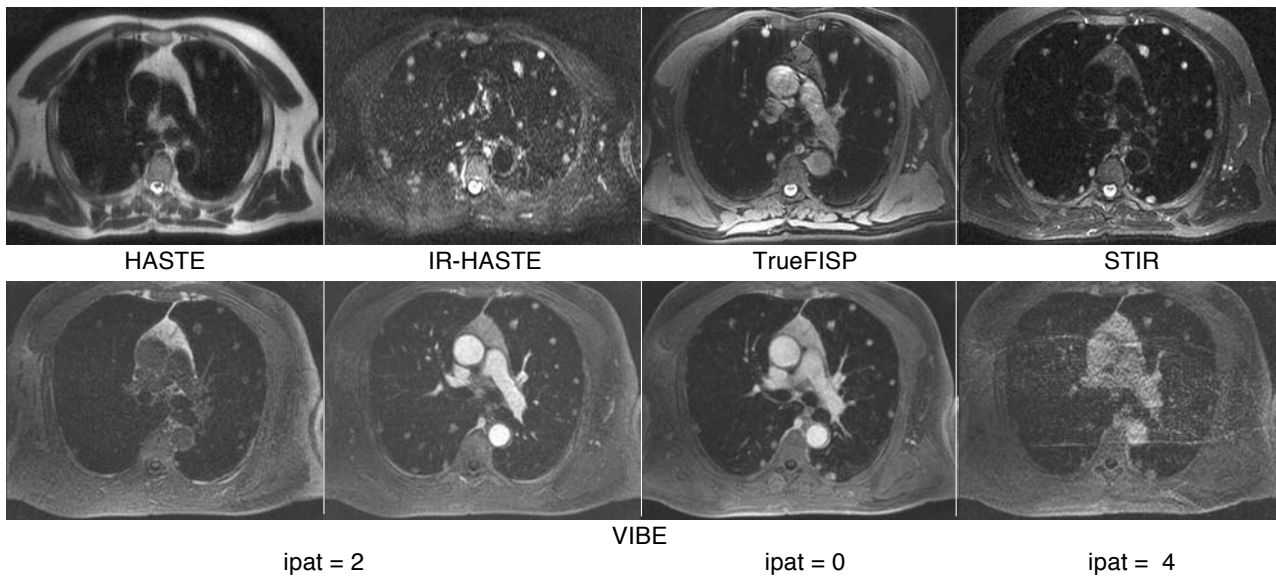


Fig. 2. Lung metastases from parotid cancer. Comparison of different MRI sequences (Table 1). The STIR- and True-FISP sequences showed the highest contrast-to-noise ratio (CNR), sensitivity and quality in the depiction of the lung metastases. In this case, the many nodules > 5 mm were excluded to simplify the analysis.

optimal placement of the ROI, nodules were maximally magnified. In this manner, partial volume artefacts in the ROI-measurement were reduced. The diameter of the nodules was measured on maximally magnified CT images.

The MRI sequences were compared in a non-blinded fashion by a lesion-to-lesion comparison (a) quantitatively in terms of the contrast-to-noise ratio (CNR) of the nodules to the adjacent lung (paired t-test) and (b) qualitatively in terms of the visualization of nodules with a diameter ≤ 10 mm relative to CT. The CNR was rated zero if a nodule was not visualized. The quality in the visualization of lung nodules was rated relative to CT on a four point scale (not, worse, similar or better depicted than in CT). Moreover, additional findings revealed by the MRI were also documented.

RESULTS

52 lung nodules were analyzed: 6 lung cancer (mean size: 43 ± 30 mm, range: 16-97 mm) and 46 metas-

in size. 8 were too small for ROI measurements and therefore excluded from the CNR analysis.

The results of the lesion-to-lesion comparison are summarized in the Figures 3 and 4. The STIR sequence significantly (p<0.01) showed the highest CNR in the visualization of malignant lung nodules followed by the FS TrueFISP, CE VIBE_{ipat = 0}, CE VIBE_{ipat = 2}, IR-HASTE, HASTE, CE VIBE_{ipat = 4}, and VIBE. The STIR sequence depicted 17 of 25 lung nodules ≤ 5 mm (68%) better than CT (Fig. 5).

The 19 mm benign nodule was nearly invisible on the STIR-sequences (CNR_{STIR} = 0.5, CNR_{IR-HASTE} = 0.75). It showed the highest CNR on the TrueFISP, VIBE and HASTE (CNR_{TrueFISP} = 11, CNR_{VIBE} = 2.5, CNR_{CE-VIBE} = 2.5, CNR_{HASTE} = 1.9) and only a small rim enhancement explainable by attracted atelectatic lung (Fig. 6).

The STIR images revealed additional findings that included: 4 liver lesions (3 cysts, 1 hemangioma) in one patient that could not be specified in the CT and bone metastases in two patients, which were

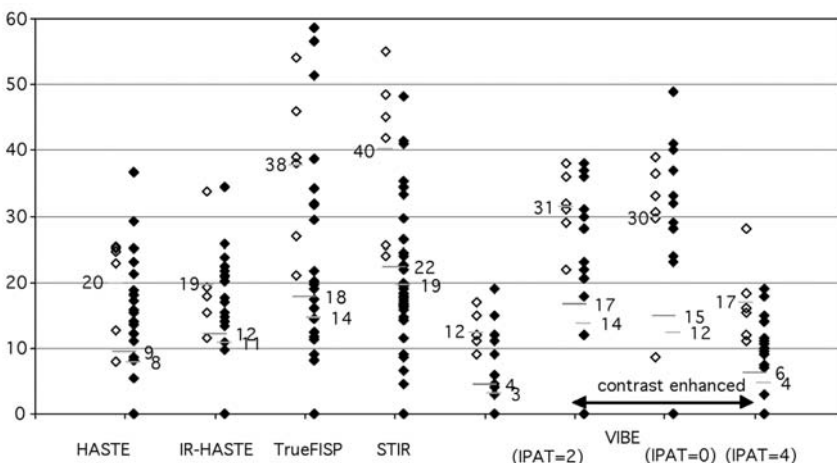


Fig. 3. Contrast-to-noise ratio (CNR) between malignant lung nodules and normal lung separated in 6 lung carcinomas (white rhombus) (mean size: 43 ± 30 mm) and 38 metastases (black rhombus) (mean size: 8 ± 7 mm). The CNR was rated zero if a nodule was not visualized.

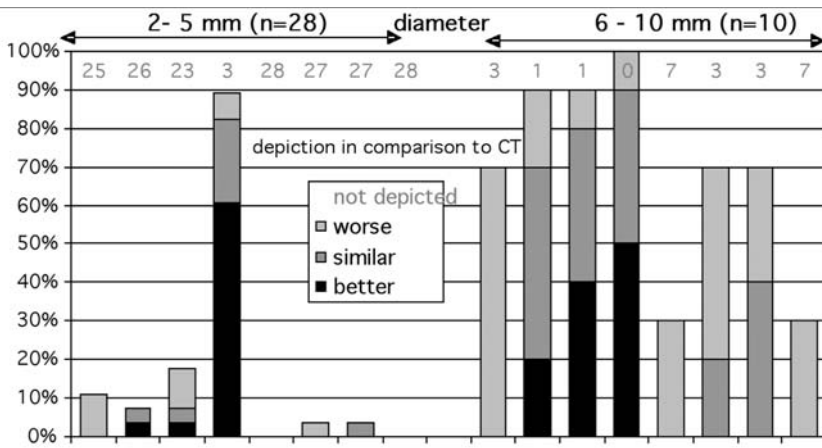


Fig. 4. Quality in the visualization of malignant lung nodules relative to multidetector CT in relation to the tested sequence and the size of the nodule (≤ 5 mm, 6-10 mm).

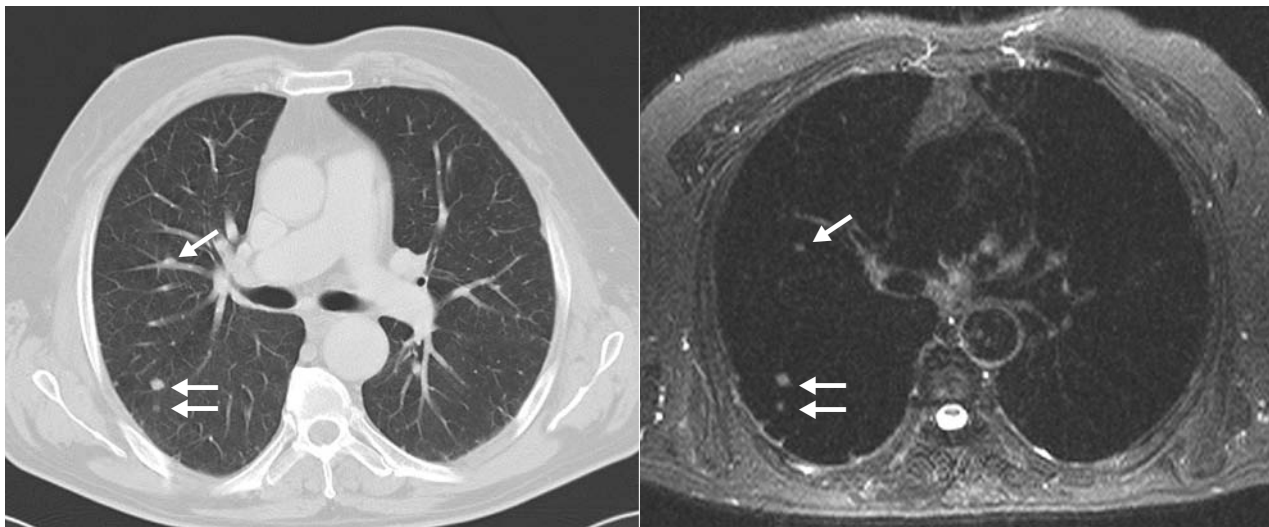


Fig. 5. Metastases from colorectal cancer (arrows). Example of malignant lung nodules that were better depicted on the STIR images than in CT.

missed in the CT and influenced the therapy planning.

DISCUSSION

In our study, we assessed MRI sequences according to their value in visualizing malignant lung nodules. Despite the limited number of patients included in this study, the STIR sequence could clearly be identified as the optimal sequence, showing the best results when considering CNR, sensitivity, and quality in visualizing malignant lung nodules. This is in accordance to a study performed with a 0.5 T scanner on 11 patients in 1992 [6]. Among all MRI sequences, the STIR sequence had the highest sensitivity for detecting malignant nodules (82%). The superiority of the STIR sequence over the other sequences in the detection of lung malignancies fits in the concept of whole body STIR-imaging [4, 5, 11, 12, 16, 21], which currently can be performed in less than 15 breathhold intervals. The FS TrueFISP sequence was found to be the second best sequence for detecting malignant lung nodules and can be used as scout to simultaneously increase the diagnostic confidence.

The non-contrast-enhanced VIBE appears to not be diagnostically useful in the detection of malignant lung nodules. The administration of contrast material in the VIBE clearly enhanced the depiction of malignant lung lung nodules but showed poorer results than the STIR or TrueFISP sequences (Fig. 1-4). Hence, both the VIBE and CE VIBE can be omitted in the MRI protocol for detecting lung malignancies. Based on the analysis of the signal intensity the STIR-sequence enables even differentiation of lymph nodes with metastasis from those without [18]. However, the advantage of the VIBE is that it can be acquired within a single breathhold interval and that it provides a 3D data set in high spatial resolution allowing for multiplanar analysis, so that the additional value of the CE VIBE in T- and N-staging needs to be further evaluated. The TrueFisp sequence was found to be the second best sequence and allows assessment of the lung vasculature and thereby also the differentiation between lymph nodes and vessels and this without the need for contrast media application or even breath holding. However, in cases, in which iv contrast material is anyway needed like for MR mammography, a CE VIBE of the lung should be additionally performed in order to (a)

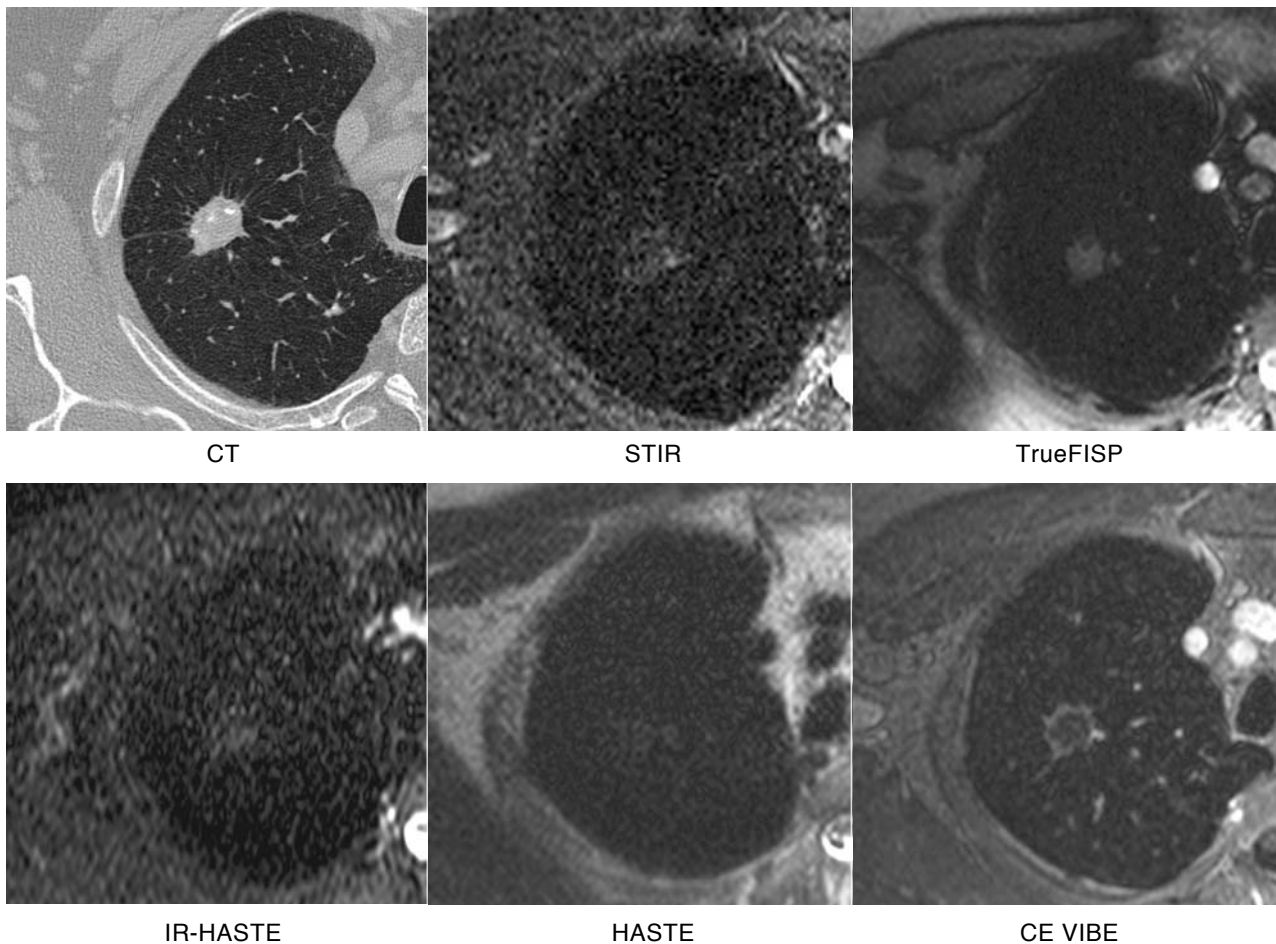


Fig. 6. Tuberculoma (resected and histologically confirmed) in a patient with mediastinal lymph nodes and adrenal masses. CT shows calcifications and scar tractions simulating spiculae surrounded by an emphysema. In MRI, there is no aspect for malignancy: no water content (edema/necrosis) and no perfusion. The contrast enhancement in the transitional zone between the nodule and normal lung can be explained through atelectatic lung caused by the scar traction.

compensate for possible misregistration artifacts between the 6 breathhold acquisitions currently needed for the STIR sequence and (b) better assess the lymph nodes by multiplanar analysis. Cardiac and vessel pulsation artefacts predominating on T1-weighted GRE [2] were eliminated on the VIBE-sequence, when an accelerating (ipat) factor ≤ 2 is used. An accelerating factor of 4 rendered the images non diagnostic.

Besides the determination of the optimal MRI sequence for detecting lung malignancies, the study also demonstrated the performance of current lung MRI in comparison to high resolution CT. The STIR sequence visualized nodules ≤ 5 mm in size – most of them even better than the CT (Fig. 4, 5). In light of higher spatial resolution, however, CT was superior in visualizing nodules ≤ 3 mm as observed in the patient with lung metastases from thyroid cancer. But without the analysis of the corresponding multiplanar reconstructions, it would have been very difficult to distinguish these tiny metastases from cross-sectioned vessels. MRI compensates its lower spatial resolution through its higher contrast. On the STIR sequence, the nodules could readily be identified as “spots in the dark lung” (Fig. 2 and 5). In contrast to CT, there are no vessels or septae superimposed on the STIR images to ham-

per the analysis, which explains why 17 of 25 nodules ≤ 5 mm were depicted better on the STIR images than in CT with higher spatial resolution (Fig. 5). The same applies to the VIBE: despite higher spatial resolution than the STIR sequence, it is disadvantaged by the superimposition of lung vessels. On STIR images the pathology is embedded in the signal void of the aerated normal lung. The signal void in the lung results from partial volume averaging with surrounding air. Increasing the spatial resolution reduces partial volume averaging and consequently increases the intensity of the background signal (lung tissue and noise). On the other hand, increasing the spatial resolution reduces the voxel size, thereby, the number of protons within a voxel and consequently the signal intensity of the nodule. Both effects, the decrease in the nodule signal and increase in the background signal lower the CNR. Therefore, it appears advisable not to reduce the slice thickness in the STIR sequence under the size of the nodule desired to be detected. The high signal intensity of malignant nodules in conjunction with the isolation through surrounding “dark” air enables separation (segmentation) of “malignant” voxels which facilitates the automation not only of tumor detection but also in the calculation of tumor volume. The cal-

ulation of tumor volume is relevant for therapy monitoring and can be supplemented by information on necrotic changes reflected by T2w imaging.

In our study, MRI revealed bone metastases, which were not demarcated in CT. Furthermore, it allowed in another patient the classification of liver lesions as cysts and hemangiomas, which would have required an ultrasound for clarification had the MRI not been performed. In the majority of organs, the higher tissue contrast renders MRI superior to CT in both, the detection and classification of pathologies. Thus, it can not be excluded that MRI can become superior to CT for staging. In the M-staging of lung cancer, for example, MRI that include brain, lung, adrenal, liver, and bone imaging could become an alternative to CT in the future – even more so when automated calculation of the tumor volume from MRI can be used for therapy monitoring. Thus, the radiological evaluation of patients with lung cancer [19] can be merged into one comprehensive examination that can be performed in less than 15 minutes. The same applies to staging breast cancer [4, 21].

Another advantage of MRI is that its specificity in the differentiating benign from malignant nodules is potentially higher than in CT due to its higher sensitivity to detect pathological water content and contrast perfusion. Faced with the high incidence of benign lung nodules, it appears to be clinically more relevant to improve the specificity in the classification instead of the sensitivity in the detection of small (≤ 5 mm) nodules. Evaluating MRI specificity is the next logical step in rendering MRI feasible for classifying lung nodules detected in x-rays or CT (Fig. 6) – or even as a first line multiorgan screening tool. Under the hypothesis that benign (scar) nodules show no significant water content and contrast enhancement [3,14,20], we expected the MRI to display only malignancies (Fig. 1 and 2 vs. Fig. 6). Contrast perfusion has been shown to be effective for distinguishing benign from malignant [3, 8, 10, 14, 17, 20]. In our study the content of water in malignancies proved to be more advantageous for visualizing nodules than contrast perfusion. Yet more research is needed to determine if the content of water is also more effective than contrast perfusion for differentiating benign from malignant nodules, possibly avoiding the need for contrast media for detection of lung nodules altogether – as suggested by our findings – and for their differentiation.

In our study, the lung carcinomas showed a higher CNR than the metastases (Fig. 3). This can be explained by the difference in size: mean size of the lung carcinoma 43 ± 30 mm vs. mean size of the metastases 8 ± 7 mm. 18 of the 36 metastases were ≤ 5 mm in size. Most of the metastases included in the CNR analysis were even 5 mm or smaller in size. In this size range, partial volume averaging with the signal void of air decreases the signal intensity when using a slice thickness of 4 mm. Therefore, 8 tiny nodules were excluded from the CNR analysis. In addition, the CNR of 3 nodules < 5 mm, not seen on the STIR images, was rated zero, which also lowered the mean CNR. The larger metastases, however seem to show the same signal intensity as the lung carcinoma included

in our study (Fig. 1 and 2). This suggests that metastases do not differ in signal from lung cancer with regards to the same size. Therefore, we deduced that small lung carcinomas would also be visualized in the same quality as the small metastases (Fig. 5). 10 of 15 lung cancer < 10 mm in diameter were detected with the VIBE in a feasibility study performed by Biederer et al. [1]. According to our study, the STIR sequence should surpass the results of the VIBE.

Limitations of the pilot study include the pragmatically approach with the sequence parameters selected in a manner to allow for breathhold imaging, the limited number of study population and the limited number of patients with benign nodules.

However, despite these limitations, the results of the pilot study – at least for lung nodules > 5 mm – warrant further investigations, if MRI with parallel imaging can compete with CT for lung screening – especially when taking into account the potentially higher specificity inherent to MRI to differentiate between benign and malignant.

REFERENCES

1. Biederer J, Both M, Graessner J, Liess C, Jakob P, Reuter M, Heller M (2003) Lung morphology: fast MR imaging assessment with a volumetric interpolated breath-hold technique: initial experience with patients. *Radiology* 226: 242-249
2. Biederer J, Reuter M, Both M, Muhle C, Grimm J, Graessner J, Heller M (2002) Analysis of artefacts and detail resolution of lung MRI with breath-hold T1-weighted gradient-echo and T2-weighted fast spin-echo sequences with respiratory triggering. *Eur Radiol* 12: 378-384. Epub 2001 Nov 27
3. Diederich S, Theegarten D, Stamatis G, Luthen R (2006) Solitary pulmonary nodule with growth and contrast enhancement at CT: inflammatory pseudotumour as an unusual benign cause. *Br J Radiol* 79: 76-78
4. Engelhard K, Hollenbach HP, Wohlfart K, von Imhoff E, Fellner FA (2004) Comparison of whole-body MRI with automatic moving table technique and bone scintigraphy for screening for bone metastases in patients with breast cancer. *Eur Radiol* 14: 99-105. Epub 2003 Jul 5
5. Eustace S, Tello R, DeCarvalho V, Carey J, Wroblecka JT, Melhem ER, Yucel EK (1997) A comparison of whole-body turboSTIR MR imaging and planar ^{99m}Tc -methylene diphosphonate scintigraphy in the examination of patients with suspected skeletal metastases. *AJR Am J Roentgenol* 169: 1655-1661
6. Feuerstein IM, Jicha DL, Pass HI, Chow CK, Chang R, Ling A, Hill SC, Dwyer AJ, Travis WD, Horowitz ME, et al (1992) Pulmonary metastases: MR imaging with surgical correlation - a prospective study. *Radiology* 182: 123-129
7. Gaa J, Rummeny EJ, Seemann MD (2004) Whole-body imaging with PET/MRI. *Eur J Med Res* 9: 309-312
8. Guckel C, Schnabel K, Deimling M, Steinbrich W (1996) Solitary pulmonary nodules: MR evaluation of enhancement patterns with contrast-enhanced dynamic snapshot gradient-echo imaging. *Radiology* 200: 681-686
9. Heidemann RM, Ozsarlak O, Parizel PM, Michiels J, Kiefer B, Jellus V, Muller M, Breuer F, Blaimer M, Griswold MA, Jakob PM (2003) A brief review of parallel magnetic resonance imaging. *Eur Radiol* 13: 2323-2337. Epub 2003 Aug 27
10. Hittmair K, Eckersberger F, Klepetko W, Helbich T, Herold CJ (1995) Evaluation of solitary pulmonary nod-

- ules with dynamic contrast-enhanced MR imaging - a promising technique. *Magn Reson Imaging* 13: 923-933
11. Iizuka-Mikami M, Nagai K, Yoshida K, Sugihara T, Suet-sugu Y, Mikami M, Tamada T, Imai S, Kajihara Y, Fukunaga M (2004) Detection of bone marrow and extramedullary involvement in patients with non-Hodgkin's lymphoma by whole-body MRI: comparison with bone and ⁶⁷Ga scintigraphies. *Eur Radiol* 14: 1074-1981. Epub 2004 Feb 18
 12. Kavanagh E, Smith C, Eustace S (2003) Whole-body turbo STIR MR imaging: controversies and avenues for development. *Eur Radiol* 13: 2196-2205. Epub 2003 Apr 25
 13. Epersjes W, Mayer E, Buchenroth M, Schunk K, Fouda N, Cagil H (1997) Diagnosis of pulmonary metastases with turbo-SE MR imaging. *Eur Radiol* 7: 1190-1194
 14. Kim JH, Kim HJ, Lee KH, Kim KH, Lee HL (2004) Solitary pulmonary nodules: a comparative study evaluated with contrast-enhanced dynamic MR imaging and CT. *J Comput Assist Tomogr* 28: 766-775
 15. Lauenstein TC, Freudenberg LS, Goehde SC, Ruehm SG, Goyen M, Bosk S, Debatin JF, Barkhausen J (2002) Whole-body MRI using a rolling table platform for the detection of bone metastases. *Eur Radiol* 12: 2091-2099. Epub 2002 Mar 8
 16. Mentzel HJ, Kentouche K, Sauner D, Fleischmann C, Vogt S, Gottschild D, Zintl F, Kaiser WA (2004) Comparison of whole-body STIR-MRI and (99m)Tc-methylene-diphosphonate scintigraphy in children with suspected multifocal bone lesions. *Eur Radiol* 9: 9
 17. Ohno Y, Hatabu H, Takenaka D, Adachi S, Kono M, Sugimura K (2002) Solitary pulmonary nodules: potential role of dynamic MR imaging in management initial experience. *Radiology* 224: 503-511
 18. Ohno Y, Hatabu H, Takenaka D, Higashino T, Watanabe H, Ohbayashi C, Yoshimura M, Satouchi M, Nishimura Y, Sugimura K (2004) Metastases in mediastinal and hilar lymph nodes in patients with non-small cell lung cancer: quantitative and qualitative assessment with STIR turbo spin-echo MR imaging. *Radiology* 231: 872-879
 19. Pugatch RD (1995) Radiologic evaluation in chest malignancies. A review of imaging modalities. *Chest* 107: 294S-297S
 20. Schaefer JF, Vollmar J, Schick F, Vonthein R, Seemann MD, Aebert H, Dierkesmann R, Friedel G, Claussen CD (2004) Solitary pulmonary nodules: dynamic contrast-enhanced MR imaging - perfusion differences in malignant and benign lesions. *Radiology* 232: 544-553. Epub 2004 Jun 23
 21. Walker R, Kessar P, Blanchard R, Dimasi M, Harper K, DeCarvalho V, Yucel EK, Patriquin L, Eustace S (2000) Turbo STIR magnetic resonance imaging as a whole-body screening tool for metastases in patients with breast carcinoma: preliminary clinical experience. *J Magn Reson Imaging* 11: 343-350

Received: July 12, 2006 / Accepted: August 7, 2006

Address for correspondence:

W. Luboldt, MD, MSc
Department of Radiology
University Hospital Frankfurt
Theodor-Stern-Kai 7
D-60590 Frankfurt am Main
Tel. +49(0)69 6301-7277
Fax +49(0)69 6301-7258
Email: luboldt@screening.info